First spectro-interferometric survey of Be stars I. Observations and constraints on the disks geometry and kinematics

Anthony Meilland, Florentin Millour, Samer Kanaan, Philippe Stee, Romain G. Petrov, Karl-Heinz Hofmann, Antonella Natta, Karine Perraut

Astronomy & Astrophysics manuscript no. Be˙AMBER˙v13
November 14, 2011

First spectro-interferometric survey of Be stars

I. Observations and constraints on the disks geometry and kinematics

A. Meilland[1], F. Millour[1], S. Kanaan[2], Ph. Stee[1], R. Petrov[1], K.-H. Hofmann[3], A. Natta[4], and K. Perraut[5]

[1] UMR 6525 CNRS H. FIZEAU UNS, OCA, Campus Valrose, F-06108 Nice cedex 2
[2] Departamento de Física y Astronomía, Universidad de Valparaíso, Chile.
[3] Max-Planck-Institut für Radioastronomie, Auf dem Hügel 69, D-53121 Bonn, Germany
[4] INAF Osservatorio Astrofisico di Arcetri, Istituto Nazionale di Astrofisica, Largo E. Fermi 5, 50125 Firenze, Italy
[5] UJF-Grenoble 1 / CNRS-INSU, IPAG UMR 5274, Grenoble, F-38041, France

Received; accepted

ABSTRACT

Context. Classical Be stars are hot non-supergiant stars surrounded by a gaseous circumstellar disk responsible for the observed infrared-excess and emission lines. The phenomena involved in the disk formation still remain highly debated.
Aims. To progress in the understanding of the physical process or processes responsible for the mass-ejection and test the hypothesis that they depends on the stellar parameters, we initiate a survey on the circumstellar environment of the brightest Be stars.
Methods. To achieve this goal, we used spectro-interferometry, the only technique combining high spectral (R=12000) and high spatial ($\theta_{\rm min}$=4 mas) resolutions. Observations were carried out at Paranal observatory with the VLTI/AMBER instrument. We concentrate our observations on the Brγ emission line to be able to study the kinematics within the circumstellar disk. Our sample is composed of eight bright classical Be stars : α Col, κ CMa, ω Car, p Car, δ Cen, μ Cen, α Ara, and o Aqr.
Results. We managed to determine the disk extension in the line and the nearby continuum for most targets. We also constrained the disk kinematics showing that it is dominated by rotation with a rotation law close to the Keplerian one. On the other hand, our survey also suggests that these stars are rotating below their critical velocities (V_c) with a mean rotational rate of 0.82±0.08 V_c
Conclusions. We did not detect any correlation between the stellar parameters and the structure of the circumstellar environment. Moreover, it seems that a simple model of a geometrically thin Keplerian disk can explain most of our spectrally-resolved K-band data. Nevertheless, some small departures from this model have been detected for at least two objects (i.e, κ CMa and α Col). Finally, our Be stars sample suggests that rotation alone cannot explain the origin of the Be phenomenon and that other mechanisms are playing a non-negligible role in the ejection of matter.

Key words. Techniques: high angular resolution – Techniques: interferometric – Stars: emission-line, Be – Stars: winds, outflows – Stars: individual (α Col, κ CMa, ω Car, p Car, δ Cen, μ Cen, α Ara, o Aqr) – Stars: circumstellar matter

1. Introduction

Classical Be stars are hot non-supergiant stars that have at least exhibited once the so called "Be-phenomenon", i.e. Balmer lines in emission and IR-excess originating from a dense gaseous circumstellar environment. A generally accepted scheme is the presence of two distinct regions in the envelope : a dense equatorial disk dominated by rotation and responsible for most of the line emission and IR-excess and a more diluted radiatively driven polar wind (Lamers & Waters 1987) with terminal velocities on the order of several hundreds of km.s^{-1} (Marlborough 1982).

However, the physical process or processes responsible for the mass-ejection and reorganization of matter in the circumstellar environment are still highly debated. The relative effect of rotation, radiative pressure, pulsation, and binarity still need to be quantified. For instance, classical Be stars are known to be fast-rotator, but estimation of their rotational velocities ranges from 50 to 100% of the critical velocity so that rotation alone might not explain the mass-ejection for all cases. Cranmer (2005), in a statistical study of the velocity of 462 classical Be stars, showed that the hottest Be stars (i.e., $T_{\rm eff}$ >18000K) have a large spread of rotational velocities whereas the cooler ones are more likely to be critical rotators. Moreover, Abbott (1979) showed that the radiative pressure alone can initiate mass-ejection only for the earliest Be stars. Consequently, it is not yet clear if Be stars can be considered as a homogeneous group of stars in term of mass-ejection processes (Stee & Meilland 2009).

An efficient way to test these hypotheses is to constrain the geometry and kinematics of the Be stars circumstellar environment since they mainly depend on the mechanisms responsible for the mass-ejection. This can only be done using long-baseline interferometry with sufficient spectral resolution as shown by Meilland et al. (2007a ; 2007b; 2011) using the VLTI/AMBER on the stars α Ara, κ CMa, and δ Sco or Delaa et al. (2010) using the CHARA/VEGA instrument on 48 Per and Φ Per. In a few cases, the stellar photosphere can also be resolved by the interferometer allowing measuring its flattening and inferring physical stellar parameters as for Achernar (Domiciano de Souza et al. 2003). For this specific object, a clear signature of a polar wind was also detected using the same VLTI/VINCI dataset by Kervella et al. (2006).

Before the availability of a new generation of instruments coupling high spectral and spatial resolutions, interferometric studies were conducted in photometric bands to measure exten-

Send offprint requests to: ame@oca.eu

Table 1. Be stars observed in this survey and their stellar parameters taken from the literature or estimated from the fit of the SED.

Name	HD	m_K (mag)	spectral class	distance (pc)	T_{eff} (K)	v sin i (km s^{-1})	V_c (km s^{-1})	pol. angle (deg)	estim. $R_\star$ ($R_\odot$)	estim. F_{env} (in the K band)
α Col	37795	2.8	B7IV	80±2	12963±203	192±12	355±23	109	5.8	0.25
κ CMa	50013	3.5	B1.5V	202±5	24627±590	244±17	535±39	106	5.9	0.47
ω Car	89080	3.5	B8III	105±1	11720±431	245±13	320±17	38	6.2	0.20
p Car	91465	3.2	B4V	148±9	17389±415	285±20	401±28	68	6.0	0.45
δ Cen	105435	2.7	B2IV	127±8	22360±589	263±14	527±29	137	6.5	0.45
μ Cen	120324	4.0	B2IV-V	155±4	22554±661	166±10	508±32	-	5.5	0.37
α Ara	158427	2.5	B3IV	82±5	18044±310	305±15	477±24	166	5.5	0.56
o Aqr	209409	4.6	B7IV	133±4	12942±402	282±20	391±27	6	4.0	0.31

sion and flattening of the circumtellar environments of many Be stars. For instance, γ Cas and ψ Per were observed by Tycner et al. (2006) with the NPOI interferometer in the Hα domain. They found that a uniform disk or a ring like model were inconsistent with their data **whereas a Gaussian model was fitting well the measurements**. γ Cas disk was also consistent with the orbital parameters already published. Nevertheless, higher-precision binary solutions were mandatory to test for a possible disk truncation by the secondary. The disk of ψ Per was found to be truncated by the presence of a companion as already predicted by Waters (1986).

γ Cas, ψ Per, ζ Tau and κ Dra were also observed with the CHARA interferometer in the K-band by Gies et al. (2007). They found, using Gaussian elliptical fits of visibilities, that the disk size in the K-band was smaller than in Hα due to a larger Hα opacity and relatively larger neutral hydrogen fraction with increasing disk radius. All these Be stars are known binaries and this binarity effect was found to be more important for ψ Per and κ Dra.

Tycner et al. (2008) using the NPOI interferometer observed χ Oph and obtained a good fit of the Hα emitting disk with a circularly symmetric Gaussian favoring the hypothesis that this object is seen under a very low inclination angle.

Using the mid-infrared VLTI/MIDI instrument, Meilland et al. (2009) have observed 7 classical Be stars between 8 and 12 they found that the size of the disk do not vary strongly with wavelength within this spectral domain which is a very different conclusion compared to B[e] with increasing sizes as a function of wavelength (Millour et al, 2009, Meilland et al. 2010, Borges Fernandes et al. 2011). Moreover the size of α Arae's disk was found to be identical at 2, 8 and 12 μm which might be due to a disk truncation by a companion. Finally it seems from their studies that disks of late type Be stars might be smaller than for early type.

Long baseline interferometry is also a powerful technique to detect companions as evidenced in Meilland et al. (2008) for the Be star δ Cen and Millour et al. (2009) for the B[e] star HD 87643. Moreover, in a theoretical study of the formation and dissipation of Be stars equatorial disks, Meilland et al. (2006) showed that interferometric follow-up of these events is the best suited technique to deduce the physical parameters of the system. However, Kanaan et al. (2008) show that, in the case of Achernar, coupling spectroscopic follow-up and large-band interferometric observations at one epoch was enough to roughly understand the geometry and kinematics of this star.

To progress in the understanding of Be stars, we initiated an observational campaign on the brightest, closest objects using the VLTI/AMBER (Petrov et al. 2007 ; Robbe-Dubois et al. 2007) and VLTI/MIDI (Leinert et al. 2003) instruments for the southern stars and the CHARA/VEGA (Mourard et al. 2009) for the northern ones. In this paper, we present new VLTI/AMBER spectro-interferometric observations of eight classical Be stars : α Col, κ CMa, ω Car, p Car, δ Cen, μ Cen, α Ara, and o Aqr.

The paper is organized as follows. In Sect. 2, we briefly introduce each target and constrain their physical parameters from various sources in the literature. The observations and data reduction process are then presented in Sect. 3, and in Sect. 4, a qualitative analysis of the reduced data for each object is shortly drawn. Then, in Sect. 5, the data are analyzed with various "toy models". Finally, these results are discussed in Sect. 6 and a short conclusion is drawn in Sect. 7.

2. Our Be stars sample

Considering the actual limiting magnitude of the VLTI/AMBER instrument, i.e. H=K=5 for an unresolved source observed with the 1.8m auxiliary telescopes in medium or high spectral resolution modes, about 30 classical Be stars are observable. However, in order to efficiently constrain the circumstellar disk kinematics, we decided to exclude targets with weak emission lines, or transient disks. Moreover, for this first survey we mainly concentrate on targets with $m_K \leq 4$. Finally, we also decide to include our first attempt to observed a fainter target, i.e. o Aqr (m_K=4.6).

Since one of our goals is to determine whether or not the Be phenomenon depends on the basic stellar parameters, we tried to select targets with the widest range of spectral classes possible. Finally, the stars selected in our sample, i.e. α Col, κ CMa, ω Car, p Car, δ Cen, μ Cen, α Ara, and o Aqr, have spectral types ranging from B1.5 to B8, and luminosity class of III, IV and V. Table 1 briefly describes the targets :

- Spectral class and the K-band magnitude (m_K) are taken from the CDS databases.
- Distance (d) is derived from van Leeuwen (2007).
- Effective temperature (T_{eff}), v sin i, and critical velocity (V_c) are taken from Frémat et al. (2005)
- Polarization measurement is taken from Yudin (2001)
- Stellar radius ($R_\star$) and K-band environment relative flux (F_{env}) are estimated by fitting the spectral energy distribution (SED) using reddened Kurucz (1979) models for stellar atmospheres using stellar parameters ($T_{\rm eff}$ and g_{eff}) from Frémat et al. (2005). The SED is first reconstructed using photometric and spectro-photometric measurements **from** the ultraviolet (IUE specta) to the far-infrared (IRAS data). To avoid contamination from the circumstellar flux, the fit of the stellar contribution to the flux is done from the ultraviolet to the visible.(see Meilland et al. 2009 for more details).

3. Observations and data reduction process

The VLTI/AMBER observations of classical Be stars presented in this paper were carried out at Paranal Observatory between

Table 2. VLTI/AMBER observing log.

Obs. time (UTC)	Telescopes conf.	Length (m)	Position angle (°)	Instrument mode	DIT (s)	Coherence (ms)	Seeing (")	Calibrators (HD)
			α Col					
2008-01-06 03:39	K0-G1-A0	88.6/ 90.5/126.2	-150.1/ -59.7/-104.3	LR-K-F	0.05	5.4	1.10	81188
2010-01-09 00:48	D0-H0-K0	60.2/ 30.1/ 90.3	51.4/ 51.4/ 51.4	HR-K-F	5.00	3.1	1.25	34642
2010-01-12 00:48	G1-D0-H0	27.3/ 50.0/ 66.6	-68.0/ -3.8/ -25.4	HR-K-F	5.00	3.9	1.06	-
2010-01-20 01:35	K0-G1-A0	90.0/ 88.7/127.5	-157.9/ -68.9/-113.8	HR-K-F	5.00	5.3	0.85	34642
2010-01-20 01:56	K0-G1-A0	89.9/ 89.6/128.0	-156.1/ -67.1/-111.7	HR-K-F	5.00	3.8	1.30	34642
			κ CMa					
2008-12-18 03:34	U1-U3-U4	102.2/ 55.6/125.3	17.1/ 96.1/ 42.9	HR-K-F	1.00	5.3	0.63	-
2008-12-18 07:32	U1-U3-U4	94.5/ 58.9/115.3	43.9/ 129.2/ 74.4	HR-K-F	1.00	4.9	0.64	-
2008-12-20 03:37	K0-G1-A0	90.5/ 81.4/121.3	-167.9/ -77.5/-125.7	LR-K-F	0.25	4.4	0.78	40805
2008-12-24 03:50	K0-G1-A0	90.5/ 84.8/124.2	-164.3/ -74.5/-121.2	LR-K-F	0.05	4.6	0.79	27442, 57299
2008-12-24 05:07	K0-G1-A0	89.9/ 90.1/128.0	-154.7/ -65.3/-109.9	LR-K-F	0.05	3.5	1.00	48305, 57299
2008-12-24 08:01	K0-G1-A0	80.9/ 82.8/102.2	-139.8/ -37.0/ -87.6	LR-K-F	0.05	5.4	0.66	48305, 57299
2010-01-09 01:39	D0-H0-K0	57.8/ 28.9/ 86.6	46.2/ 46.2/ 46.2	HR-K-F	5.00	3.1	1.26	34642
2010-01-18 00:24	H0-G0-E0	27.4/ 13.7/ 41.0	-142.8/-142.8/-142.8	HR-K-F	5.00	3.6	0.71	54173
			ω Car					
2008-12-21 04:49	K0-G1-A0	74.2/ 72.9/128.0	175.8/-125.0/-154.9	HR-K-F	5.00	3.8	0.78	75063, 69596
2008-12-21 07:37	K0-G1-A0	72.1/ 83.0/126.6	-156.4/ -85.7/-118.2	HR-K-F	5.00	3.4	0.89	69596
2008-12-24 06:33	K0-G1-A0	73.7/ 79.3/127.7	-167.4/-100.5/-132.6	LR-K-F	0.05	3.0	1.20	98134, 57299
			p Car					
2008-12-23 07:31	K0-G1-A0	79.3/ 82.3/127.8	-161.2/ -85.7/-122.7	MR-K-F	1.00	3.3	1.11	94286, 69596
2009-03-22 03:59	K0-G1-A0	71.7/ 89.6/120.8	-138.0/ -54.4/ -90.6	MR-K-F	1.00	6.0	0.70	94286
			δ Cen					
2009-03-21 04:18	K0-G1-A0	83.9/ 87.9/127.4	-153.8/ -69.5/-110.4	MR-K-F	1.00	10.9	0.74	110458
2010-01-20 08:12	K0-G1-A0	84.1/ 87.7/127.5	-154.5/ -70.4/-111.4	LR-HK	0.05	2.6	1.27	110458
2011-05-19 02:41	U1-U2-U4	46.4/ 82.3/111.4	43.8/ 106.6/ 84.8	LR-HK	0.025	1.3	1.47	103513
			μ Cen					
2011-06-26 23:21	K0-A1-G1	128.9/ 78.1/ 88.2	-121.5/ 100.6/-157.9	HR-K-F	6.00	1.6	0.90	128488
2011-06-30 00:19	D0-I1-G1	82.3/ 44.5/ 70.8	104.8/-134.5/ 137.5	HR-K-F	5.00	3.4	0.94	128488
			α Ara					
2007-07-28 05:51	G1-D0-H0	71.5/ 44.7/ 55.4	-5.4/ 123.9/ 33.3	LR-K	0.025	3.5	0.44	177716, 164371
2007-04-13 05:47	H0-G0-E0	30.8/ 15.4/ 46.3	-143.4/-143.4/-143.4	LR-K	0.025	3.0	0.63	124454
2007-06-09 07:11	K0-G1-A0	74.2/ 90.0/112.3	-135.8/ -41.6/ -82.8	LR-K	0.025	2.7	0.57	166460, 164371
2007-06-09 08:02	K0-G1-A0	68.3/ 88.9/102.5	-130.4/ -30.7/ -71.7	LR-K	0.025	1.6	0.95	166460, 164371
2007-06-06 07:30	K0-G1-A0	72.5/ 89.6/109.5	-134.2/ -38.5/ -79.7	LR-K	0.025	1.3	1.38	124454, 164371
2007-06-06 08:50	K0-G1-A0	63.4/ 88.0/ 95.0	-126.9/ -22.7/ -63.0	LR-K	0.025	1.3	1.42	164371
2007-04-14 06:22	H0-G0-E0	31.4/ 15.7/ 47.2	-133.5/-133.5/-133.5	LR-K	0.025	2.9	0.67	164371
2007-05-16 07:34	H0-D0-A0	61.1/ 30.6/ 91.7	-96.4/ -96.4/ -96.4	LR-K	0.025	3.0	1.25	124454, 164371
2007-06-10 07:44	K0-G1-A0	70.2/ 89.2/105.7	-132.0/ -34.1/ -75.2	LR-K	0.025	2.3	0.58	164371, 21201
2007-05-17 02:34	H0-D0-A0	60.2/ 30.1/ 90.3	-156.3/-156.3/-156.3	LR-K	0.025	3.0	0.79	124454
2007-05-17 09:53	H0-D0-A0	49.3/ 24.6/ 73.9	-67.2/ -67.2/ -67.2	LR-K	0.025	1.9	1.53	164371
2011-06-30 02:04	D0-I1-G1	78.2/ 45.8/ 62.7	82.6/-150.7/ 118.4	HR-K-F	5.00	3.7	0.85	163145, 152786
2011-06-30 03:03	D0-I1-H0	81.4/ 37.2/ 63.8	93.9/ -36.5/ 67.6	HR-K-F	5.00	2.9	1.08	163145, 152786
2011-06-30 03:37	D0-I1-H0	82.2/ 38.1/ 63.2	100.4/ -31.9/ 73.9	HR-K-F	5.00	2.9	1.05	163145, 152786
2011-06-30 04:28	D0-I1-H0	82.0/ 39.0/ 61.2	110.1/ -24.7/ 83.3	HR-K-F	5.00	2.4	1.27	163145, 152786
2011-06-30 05:03	D0-I1-H0	81.0/ 39.4/ 58.9	117.5/ -19.2/ 90.2	HR-K-F	5.00	2.9	1.03	163145, 152786
2011-06-30 06:00	D0-I1-H0	78.5/ 39.8/ 54.4	129.4/ -10.7/ 101.3	HR-K-F	5.00	2.9	1.02	163145, 152786
2011-06-30 06:38	D0-I1-H0	76.4/ 39.9/ 50.6	138.1/ -4.7/ 109.7	HR-K-F	5.00	3.2	0.92	163145, 152786
			o Aqr					
2011-06-30 10:08	D0-I1-H0	67.4/ 34.3/ 58.8	102.8/ -16.5/ 72.2	HR-K-F	5.00	2.9	1.02	209926

2007 and 2011. Most observations were executed using the 1.8 meters movable auxiliary telescopes (AT), a few others were made using 8.0m unit telescopes (UT). The VLTI/AMBER observing log for the eight targets and their corresponding interferometric calibrators are presented in Table 2. The (u,v) plan coverage for each target is plotted in Fig 1.

Since the observations were spread over a long period of time, starting soon after the opening of AMBER to the scientific community, the data are quite inhomogeneous, both in term of quality and observing modes. AMBER offers three different spectral dispersion modes : the low-resolution (LR) with R=$\lambda/\delta\lambda\simeq$35, the medium-resolution (MR) with R$\simeq$1500, and the high-resolution (HR) with R$\simeq$12000 . All these modes were used during our observing campaign, depending on their availability at the epoch of observations, on the brightness of the target, and on the seeing conditions. MR and HR observations were centered on the Brγ emission line to enable the study of the circumstellar gas kinematics through the Doppler effect.

Most of the data have benefited from the installation of the fringe tracker FINITO that enables longer integration time by stabilizing the fringes. The detector integration time (DIT) ranges from 25 ms for bright targets in LR mode without FINITO to several seconds for observations in HR mode with FINITO. Under good seeing conditions (i.e. seeing <0.8") the

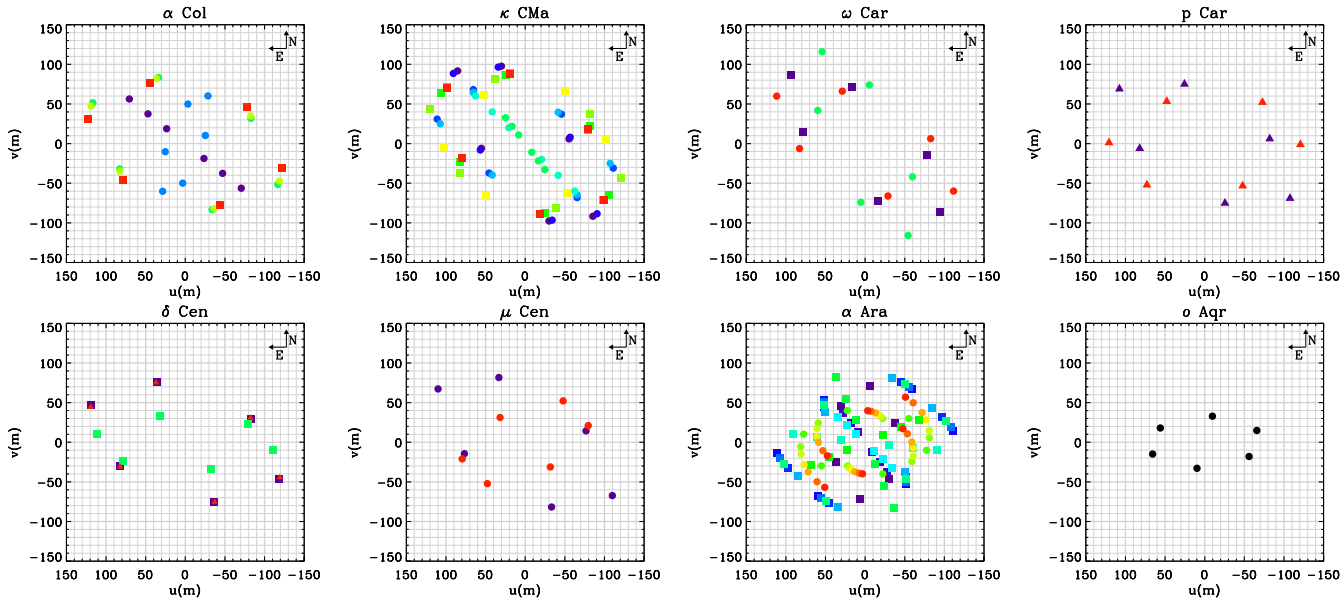

Fig. 1. (u,v) plan coverage obtained for the observed Be stars. LR mode observations are plotted as squares, MR ones as triangles, and HR ones as circles. Each observation, i.e. three baselines measurements, is plotted with a different color.

use of FINITO allows to obtain a significantly higher signal to noise ratio (SNR) both for short and long integration time, enhancing significantly the quality of the data for all observing modes.

Data were reduced using the VLTI/AMBER data reduction software, i.e., `amdlib v3.0.3b1` (see Tatulli et al. 2007 and Chelli et al. 2009 for detailed informations on the AMBER data reduction). We performed selection of individual exposures using the standard selection criteria (Millour et al. 2007). We reject 80% of frames with the lowest SNR. For observations in LR mode we also reject the frames with piston larger than 10μm as well as frames with flux ratio between the three beams higher than 3.

The interferometric observables (visibility, differential phase, and closure phase) are then averaged and calibrated. For this last step we used scripts described in Millour et al. (2007) that are now part of the standard amdlib package. The calibration process includes estimation of the calibrators' size and their uncertainties from various catalogs, determination of their transfer function and their evolution during the whole night, and computation of the calibrated visibilities and phases. The final errors on the measurements include uncertainties on the calibrators' diameter, the atmosphere transfer function fluctuations and intrinsic errors on the measurements.

4. A qualitative analysis of our dataset

The Brγ line for all the observed targets is clearly in emission (See Fig 2 and Table 3 for a summary of their main spectral characteristics). In almost all cases, the MR and HR data also exhibit a drop of visibility in the emission line due to a variation of the circumstellar environment extension and relative flux between the continuum and the line as already explained in Meilland et al. (2007a). They also exhibit "S" shape or more complex variations of the differential phase in the line, and HR data clearly show that some visibility variations are "W" shaped (See e.g. Fig. 3). Such characteristics are clear evidences of the presence of a rotating equatorial disk as described in Meilland et al. (2011) in the case of δ Scorpii. The MR and HR data for all targets are presented in Figs. 3 to 10.

We note that for the HR observations executed before the replacement of a disturbing optical element in front of the VLTI *InfraRed Image Sensor* (IRIS) in 2010, some instrumental modulations with a very high frequency are seen in the HR data. It is especially the case for ω Car. In order to enhance the data quality we have decided to filter these modulations using a standard Fourier-transform low-pass-filter technique.

Some targets are also partly resolved in the K-band continuum. However, considering the uncertainties on the calibrated absolute visibilities, it is difficult to determine an accurate extension of the circumstellar disk in the continuum for all the targets. Thus, in order to be more efficient we have decided to only use the differential visibility (i.e. visibility of each spectral channel divided by the mean visibility) for our kinematics study and the absolute continuum visibility to determine the K-band extension when possible.

Among our sample we did not detect any new companion, and δ Cen remains the only star for which a companion was visible in the interferometric signal as already evidenced by Meilland et al. (2008). The individual comments for the observed objects are the following :

- α Col : We have obtained 3 measurements in HR, and one in LR. The data SNR is quite high and the uncertainties on the differential quantities are on the order of a few percents. The target is clearly resolved in the line and the measurements in HR clearly exhibit the typical visibility and phase variations of a rotating disk with the major-axis roughly perpendicular to the polarization measurement obtained by Yudin 2001 (see Table 1). The quasi-symmetric double-peaked line profile indicates that the object is seen under an intermediate inclination angle and that no major inhomogeneity is present in the disk. The object is also partly resolved in the continuum, with a visibility of about 0.9±0.05 for the longest baselines.
- κ CMa : This star was observed a first time in December 2008 and we have obtained 2 measurements in HR and 5 in LR. It was observed again in January 2010 and 2 new

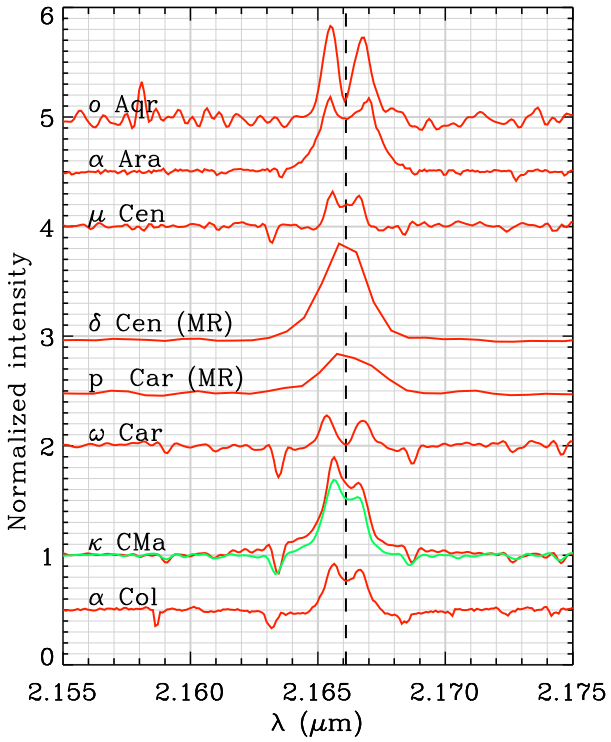

Fig. 2. Brγ spectra from our VLTI/AMBER observations. The data were taken in HR mode for all observations expect for p Car and δ Cen (MR mode). For κ CMa the red and green lines represent the 2008 and 2010 observations, respectively.

measurements in HR were acquired. The SNR is quite high except for the last observations in 2010. All the HR measurements at the two epochs show the typical visibility and phase variations of a rotating disk. The disk major-axis seems to be roughly perpendicular to the polarization measurement. The double-peaked line profile and some visibility and phase variations are strongly asymmetric. These asymmetries probably stems from the presence of an inhomogeneity in the disk that was already described in Meilland et al. (2007b). We note that the line profile V/R ratio did not significantly vary between our 2008 and 2010 observations. The LR data shows that the star is at least partly resolved in the continuum, but the calibration is not accurate enough to fully constrain the continuum extension.

- ω Car : We have obtained 2 measurements in HR and one measurement in LR. Despite the fact that the SNR is lower compared to α Col, a visibility and phase signals typical of a rotating disk are also present in the data. The major-axis does not seem to be neither aligned nor perpendicular to the polarization measurement. As the line profile is double-peaked with a narrow shell line at its center, the star is probably seen under a high inclination angle. The LR data clearly indicate that the object is partly resolved in the continuum, i.e. V~0.85 for the longest baseline. We note that the second HR measurement cannot be calibrated accurately.
- p Car : We have obtained 2 measurements in MR, both showing a bright emission line, a drop of visibility, and a "S" shape phase variations in the line. Considering the phase amplitude and the lack of spectral resolution, it is hard to qualitatively determine the position of the major-axis of the equatorial disk. We note that the profile and phase variations are asymmetric. This is probably due to the presence of an inhomogeneity such as a one-armed oscillation as proposed by Okazaki (1997). The object is barely resolved in the continuum (V~0.9 for the longest baselines).
- δ Cen : Previous VLTI/AMBER LR and MR observations published by Meilland et al. (2008) evidenced the binarity of this object. The authors found a contribution of the companion to the total K-band flux of 7% and a separation of 68.7 mas. In order to check their results and constrain the system orbit, the star was observed again in 2009, 2010, and 2011. In the 2009 MR data a bright Brγ emission line, a drops of visibility and a "S" shape phase variations are clearly visible. These data as well as the 2010 LR ones also contain modulations due to the binarity of the object. We note that no obvious modulation is seen in the 2011 LR dataset. This may mean that the separation is quite small, on the order of a few milli-arcseconds.
- μ Cen : We have obtained 2 measurements in HR. Since this target is quite faint, i.e., m_K=4, the SNR is low. However, "S" shape variations are still clearly present in the differential phases. We also detect a drop of visibility for one baseline, whereas it is clearly below the noise level for the other ones. The line profile is double-peaked and symmetric. The fact that the line intensity is quite low, i.e. 1.3 times the continuum, contributes to the weakness of the visibility drop. The object is unresolved in the continuum.
- α Ara : This star was observed 11 times in LR mode in 2007 but the data quality was too low to obtain more than an estimation of the disk extension (see Sect. 5.1). More recently, we have observed α Ara again during one full night and obtained 7 measurements in HR mode. All data exhibit a clear signature of a rotating disk, with a major-axis roughly perpendicular to the polarization measurement and compatible with Meilland et al. (2007a) results. The profile is double-peaked and symmetric. The object is partly resolved in the continuum for all baselines, however due the unstable weather conditions during the observing night, the uncertainties on the absolute visibility remains on the order of 20%.
- o Aqr : This is the faintest target of our sample with m_K=4.6. We have obtained 1 measurement in HR mode. The SNR is very low, and we were close to the instrumental sensibility limit considering the quite bad weather conditions during the observations (seeing of 1" and coherence time of less than 3ms). However, a "S" phase signal is still clearly visible in the data, at least for the longest baseline. Clues of a small drop of visibility in the line are also present. The profile is typical of Be stars seen at high inclination angle, i.e. double-peaked with a shell absorption line at its center. The object is clearly unresolved in the continuum.

Table 3. Brγ line characteristics

Star	EW Å	Peaks separation Å (km s^{-1})	V/R	Remarks
α Col	6.1	9.9 (138)	1.04	-
κ CMa(2008)	16.8	9.9 (138)	1.13	-
κ CMa(2010)	11.6	10.4 (144)	1.10	-
ω Car	3.5	14.2 (196)	1.04	Be-Shell
p Car	8.2	~15 (200)	>1	MR obs.
δ Cen	17.9	~15 (200)	~1	MR obs.
μ Cen	3.7	10.4 (144)	1.03	-
α Ara	16.0	15.1 (209)	1.01	-
o aqr	12.6	12.8 (177)	1.00	Be-Shell

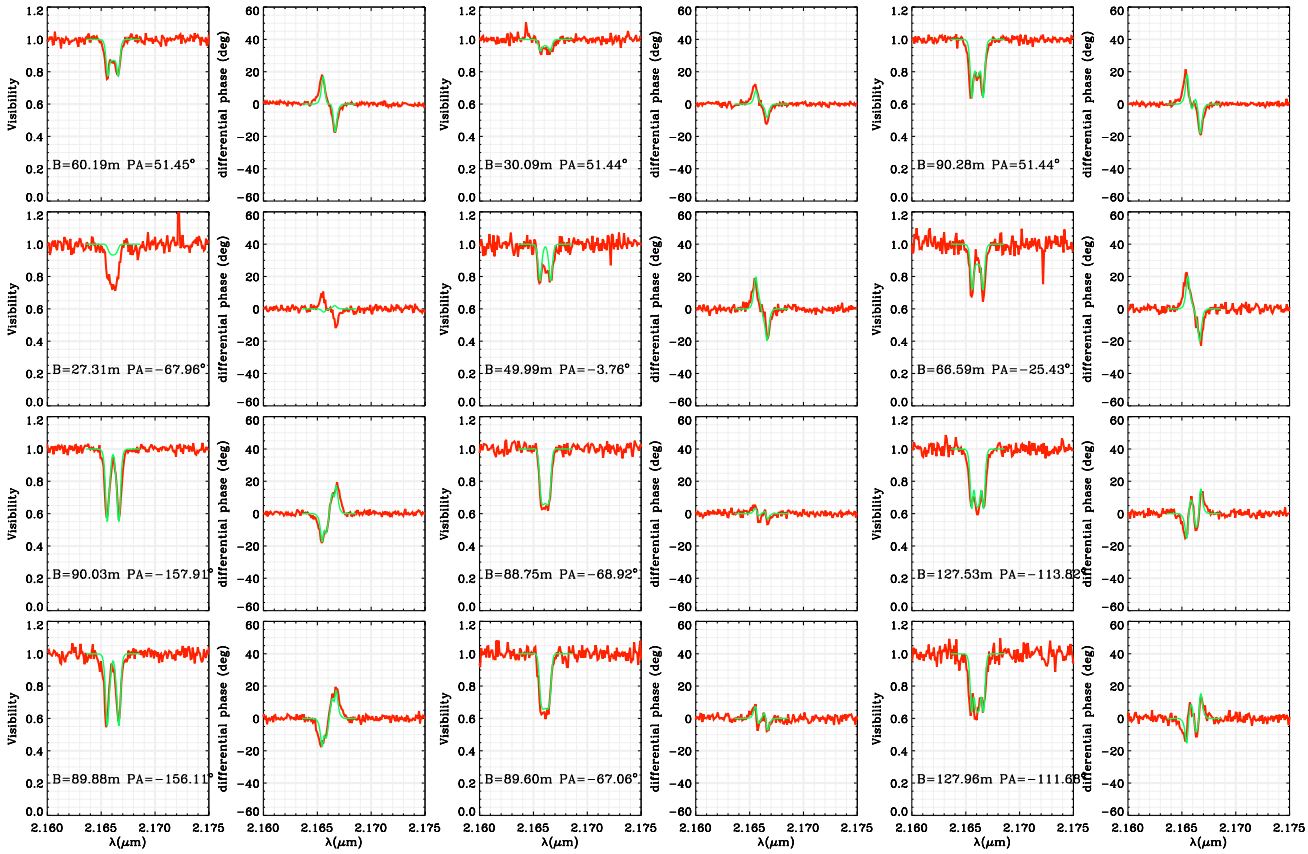

Fig. 3. α Col differential visibility and phase from our 4 VLTI/AMBER HR measurements (red line). Each row corresponds to one VLTI/AMBER measurement (3 different baselines). The visibility and phase of the best-fit kinematics model is overplotted in green.

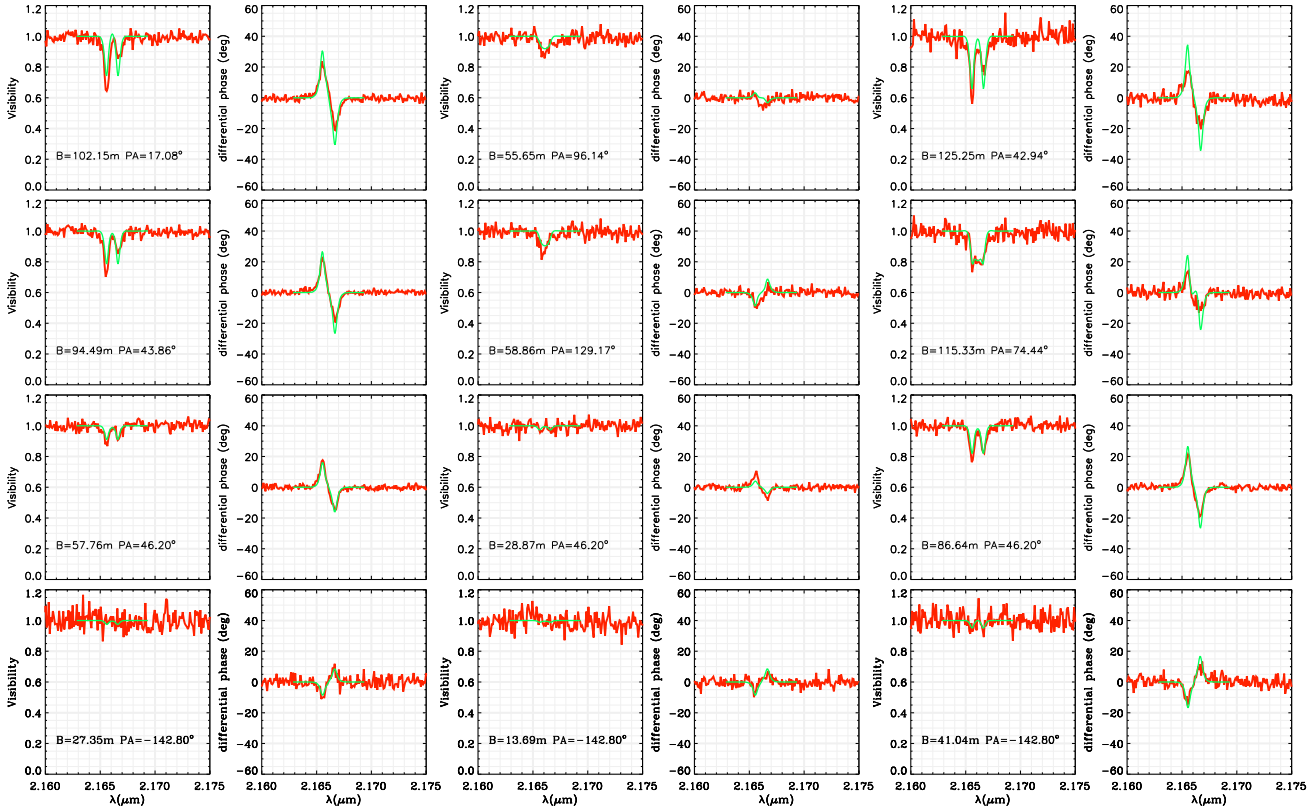

Fig. 4. κ CMa visibility and phase from our 4 VLTI/AMBER HR measurements (red line). The two first measurements are from 2008 (first two row) and the two other from 2010. The best-fit kinematics model is overplotted in green.

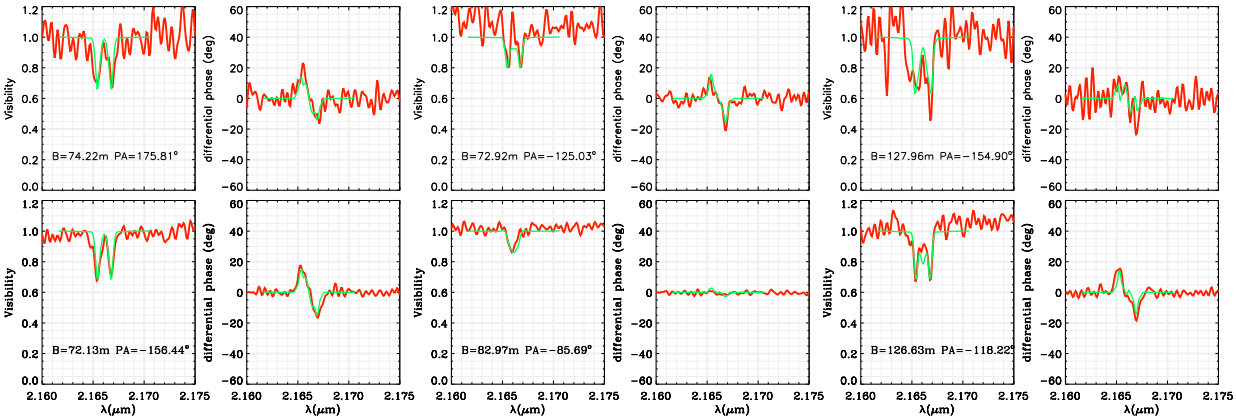

Fig. 5. ω Car visibility and phase from our 2 VLTI/AMBER HR measurements (red line). The best-fit kinematics model is overplotted in green.

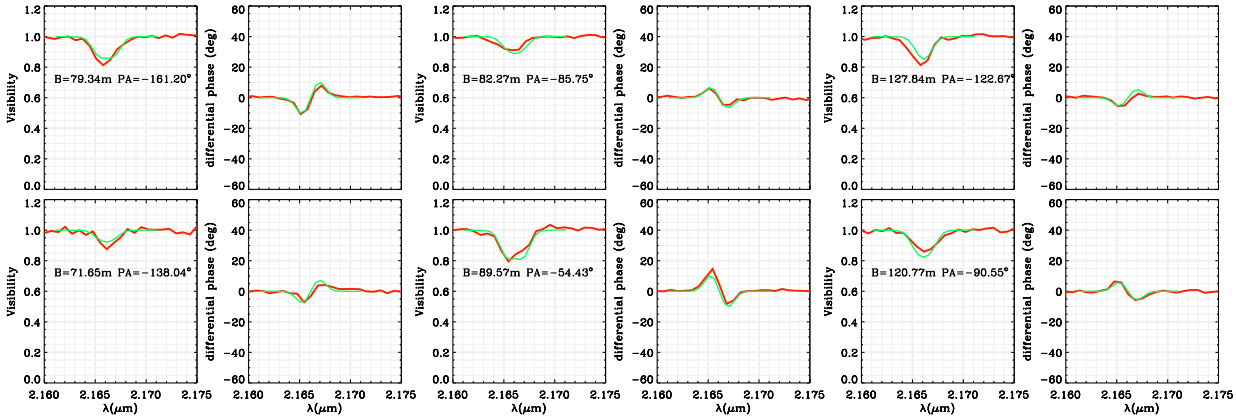

Fig. 6. p Car visibility and phase from our 2 VLTI/AMBER MR measurements (red line). The best-fit kinematics model is overplotted in green.

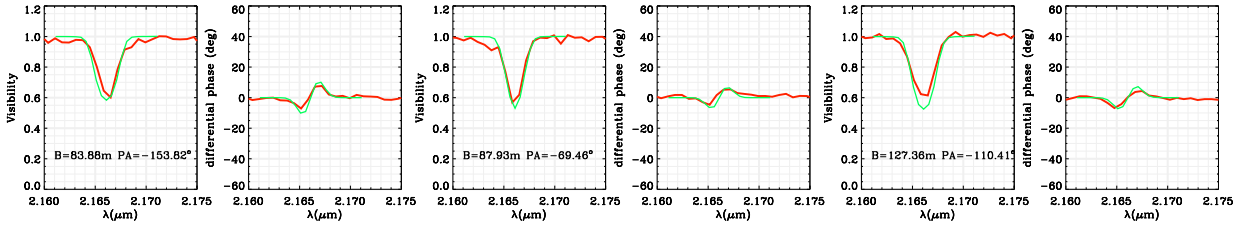

Fig. 7. δ Cen visibility and phase from our VLTI/AMBER HR measurement (red line). The best-fit kinematics model is overplotted in green.

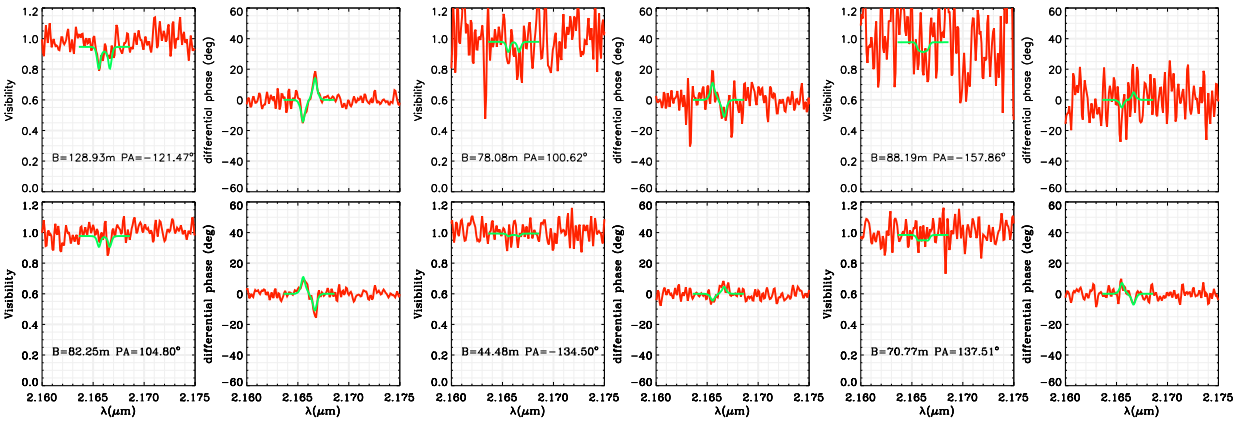

Fig. 8. μ Cen visibility and phase from our 2 VLTI/AMBER HR measurements (red line). The best-fit kinematics model is overplotted in green.

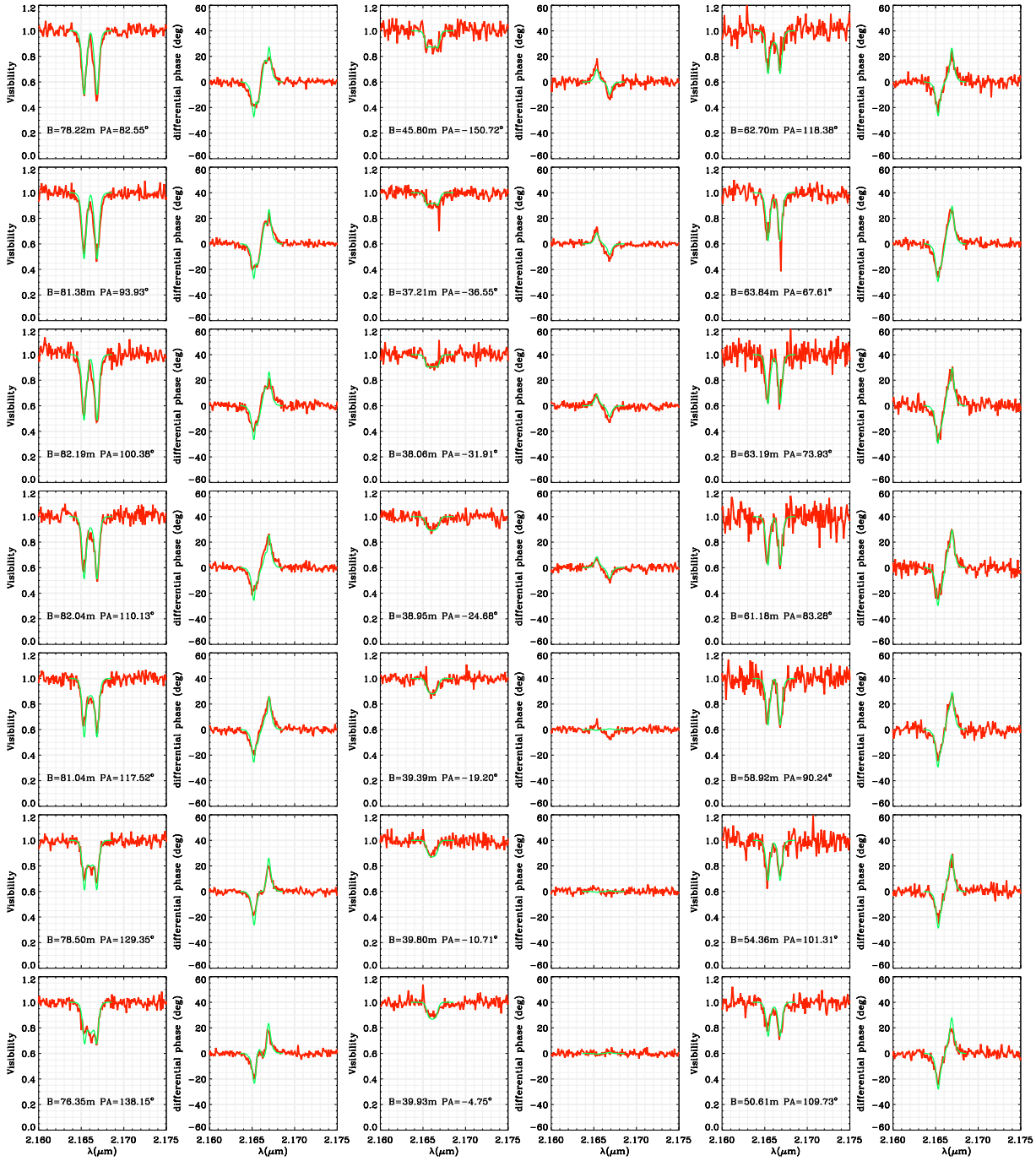

Fig. 9. *α* Ara visibility and phase from our 7 VLTI/AMBER HR measurements (red line). The best-fit kinematics model is overplotted in green.

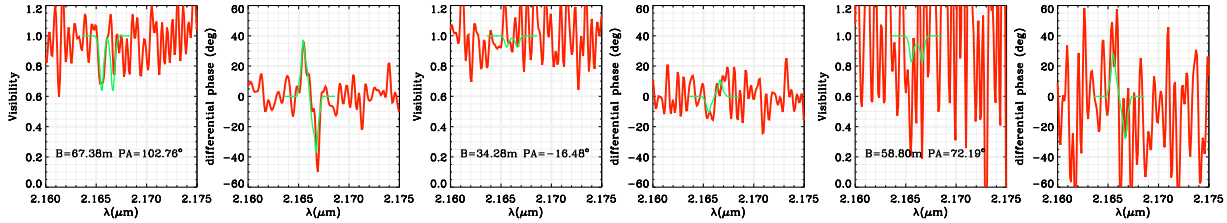

Fig. 10. *o* Aqr visibility and phase from our VLTI/AMBER HR measurement (red line). The best-fit kinematics model is overplotted in green.

5. Modeling

In this section we analyzed our interferometric data using "toy models" of increasing complexity. In the first subsection the K-band continuum visibility is used to estimate the circumstellar environment extension. In the case of the Be binary star δ Cen we tried to constrain the components separation at various epochs. Finally, in the last subsection, the differential visibility and phase are used to constrain the circumstellar environment's kinematics.

5.1. The disk extension in the continuum

To estimate the circumstellar disk extension in the K-band continuum using our interferometric measurements, we used a simple two components model. As all the central stars are unresolved or barely resolved even with the longest baselines (i.e. V>0.95) they were all modeled as point sources. The second contribution is the circumstellar environment. Due to the large uncertainties on most of our absolute visibility measurements we were not able to determine any flattening of the environment and we decided to simply model this contribution as a circular Gaussian distribution. For the same reason, we decided to set the circumstellar environment relative flux (F_{env}) to the value determined from the fit of the SED with a much higher precision than if it was deduced from the interferometric data only (See Section 2 and Table 1). Finally, the two-dimensional intensity map **describing** our model is given by :

$$I(x,y) = (1 - F_{env})\delta(x,y) + \frac{F_{env}}{\sigma\sqrt{2\pi}} exp\left(-\frac{x^2+y^2}{2\sigma^2}\right) \quad (1)$$

where x and y are the Cartesian coordinates, δ(x,y) is the Dirac function, and σ is the standard deviation of the Gaussian distribution. In the following, the Gaussian distribution is not defined by its standard deviation but by its full width at half maximum defined by FWHM$\simeq 2.35\sigma$.

For each dataset, we have separated the low-spectral resolution data from the medium or high-resolution data and fitted the above-described models. The results are summarized in Table 4. In most cases, we see that the accuracy of the LR data is higher than MR or HR, but that larger biases affect them. Few cases were very problematic and no relevant fit to the data could be obtained. These special cases are marked as "n. c." for "not constrained" in this table.

Using the distance and stellar radius from Table 1 we could infer the extension in $D_\star$. These values, also presented in Table 4, clearly show that the K-band continuum is quite compact. However, because of the large uncertainties on our measurements, we could not determine whether or not the K-band extension depends on any stellar parameters. Nevertheless, we could determine a mean size of the environment, i.e. $\overline{\text{FWHM}} = 2.2 \pm 0.3\, D_\star$ for the whole dataset.

α Ara and κ CMa were already observed with the VLTI/AMBER and modeled by Meilland et al. (2007a, 2007b). For α Ara, the authors found a mean continuum K-band extension of 6.0±0.8 mas thus significantly larger than our 2.4±1.1 mas measurement. However, their modeling was done using uniform disk component for the environment. Thus, as the environment is not fully resolved we have to apply a x0.87 correcting factor to their measurements to convert the uniform disk diameter into a Gaussian FWHM. Nevertheless, this 6.0x0.87=5.3±0.7 mas is still significantly larger than our measurement (>2σ). In the case of κ CMa, the authors found that the mean K-band continuum extension was smaller than 2.7 mas which is compatible with our 1.0 ± 0.3 mas extension.

Table 4. The K-band continuum extensions of the disks.

Name	F_{env} (fixed)	Gaussian FWHM mas	$D_\star$	χ^2_r
α Col (HR)	0.25	1.3 ± 0.7	1.5±0.8	0.7
α Col (LR)	0.25	1.0 ± 0.2	1.9±0.4	2.0
κ CMa (HR)	0.47	n.c.	n.c.	n.c.
κ CMa (LR)	0.47	1.0 ± 0.3	3.7±1.1	4.8
ω Car (HR)	0.20	n.c.	n.c.	n.c.
ω Car (LR)	0.20	1.7 ± 0.5	3.1±0.9	1.9
p Car (MR)	0.45	1.1 ± 0.3	2.0±0.5	3.1
μ Cen (HR)	0.37	n.c.	n.c.	n.c.
α Ara (HR)	0.56	2.4 ± 1.1	3.8±1.7	7.1
α Ara (LR)	0.56	1.9 ± 1.3	3.0±2.1	5.2
o Aqr(HR)	0.31	n.c.	n.c.	n.c.

5.2. The binarity of δ Cen

We separately fitted the δ Cen data with a uniform disk + a companion star model in order to compare it with Meilland et al. 2008. The two-dimensional intensity map is **given** by :

$$I(x,y) = F_\star\delta(x,y) + F_{comp}\delta(x-\Delta\alpha, y-\Delta\delta) + \frac{4\,F_{env}}{\pi D_{env}^2}\Pi\left(\frac{\sqrt{x^2+y^2}}{D_{env}}\right) \quad (2)$$

where $F_\star$, F_{comp}, and F_{env} are the stellar, companion, and environment fluxes, respectively, ($\Delta\alpha$,$\Delta\delta$) the components separation in Cartesian coordinates, and Π(t) is the rectangle function defined by Π(t)=1 for t≤1/2 and Π(t)=0 for t>1/2.

The fit procedure is similar to what was done in Millour et al. (2009), i.e. a mix of Levenberg-Marquardt descent with a set of Monte Carlo initial parameters. The only free parameters are the companion coordinates. The other parameters are set to their values determined by Meilland et al. (2008): primary flux $F_\star$=0.41, envelope flux F_{env}=0.52, companion flux F_{comp}=0.07, and envelope diameter D_{env}=1.6 mas. The results are presented in Table 5.

We find that the position of the companion varied significantly between the 4 epochs separated roughly from 1 year each. It made an almost complete revolution around the main star during this period, pointing to a typical period of the system of about 5 years. In order to constrain significantly the orbital elements the star should be observed again several times with long-baseline interferometry or speckles interferometry. These data should also be completed by radial velocity measurements.

Nevertheless, we tried to determine a first estimate of a possible orbit. It has a probably very low eccentricity but a very large inclination angle. We managed to obtain a good fit of the orbit with the following parameters : semi-major axis of 80 mas, periastron in January 2008, period of 5.2 yrs, no eccentricity, inclination angle of 81^o, $\omega = 212^o$, and $\Omega = 110^o$. We note that considering the low number of measurements and the probable low eccentricity, this possible orbit, overplotted in Fig 11, may no be unique.

Table 5. Evolution of δ Cen components separation.

Date	Cartesian coord. $\Delta\alpha$ (mas)	$\Delta\delta$ (mas)	Polar coord. sep (mas)	PA (deg)
2008-01	60.9	-31.7	68.7	117.5
2009-03	-34.5	0.79	34.5	-88.7
2010-01	-73.8	24.5	77.8	-71.6
2011-05	2.78	9.25	9.7	16.7

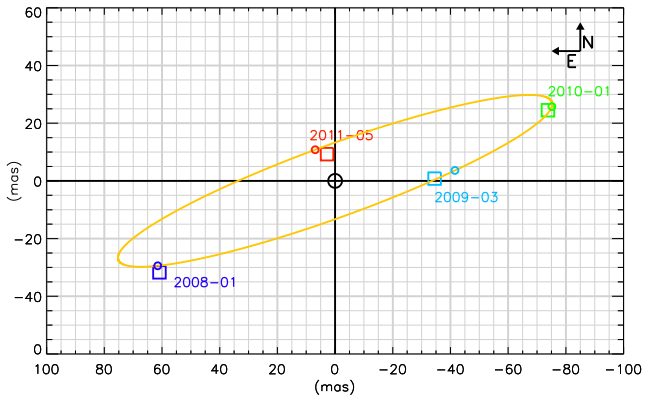

Fig. 11. δ Cen binary separation and possible orbit. The measured separations are plotted as squares. The possible orbit is plotted as an orange solid line and the circles represents the modeled positions at the epochs of observations.

5.3. The equatorial disk kinematics

5.3.1. A simple "toy" model

In order to constrain quantitatively the velocity fields in the circumstellar environment of the observed Be stars using interferometric observations, we developed a simple two-dimensional kinematic model of a rotating and/or expanding equatorial disk. This model has already been used to model three classical Be stars (see Delaa et al. 2011 and Meilland et al. 2011) and one A[e] supergiant star (Millour et al. 2011) and it is described in detail in Delaa et al. (2011). The model geometry is completely ad-hoc : the star is modeled as a uniform disk and the envelope emission in the continuum and the emission line as two elliptical Gaussian distributions of different FWHMs but with the same flattening due to a projection effect of the geometrically thin equatorial disk, i.e., $f = 1/cos(i)$, where i is the object inclination angle.

The emission maps are then combined with a two-dimensional projected velocity map of a geometrically thin expanding and/or rotating equatorial disk. For each spectral channel in the line, an iso-velocity map projected along the line of sight is then calculated and multiplied by the whole emission map in the line. Finally, the whole emission map for each wavelength consists of the weighted sum of the stellar map, the disk continuum map and the emission line map within the spectral channel under consideration (see Fig 12 for an example of emission map obtained in a narrow spectral channel).

The model parameters can be classified into 4 categories:

1. The stellar parameters: stellar radius ($R_\star$), distance (d), inclination angle (i), and disk major-axis position angle (PA).
2. The kinematic parameters: rotational velocity ($V_{\rm rot}$) at the disk inner radius (i.e., photosphere), expansion velocity at the photosphere (V_0), terminal velocity (V_∞), and exponents of the expansion (γ) and rotation (β) velocity laws.
3. The disk continuum parameters: disk FWHM in the continuum ($a_{\rm c}$), disk continuum flux normalized by the total continuum flux ($F_{\rm c}$).
4. The disk emission line parameters: disk FWHM in the line ($a_{\rm l}$) and line equivalent width (EW).

The star distance is taken from van Leeuwen (2007) and $F_{\rm c}$ and $R_\star$ are derived from the fit of the SED (see Table 1). The other nine parameters are free.

If the disk is directly connected to the stellar surface, the rotational velocity ($V_{\rm rot}$) should be equal to the stellar rotational velocity. However, in some cases, $V_{\rm rot}$ may exceed the stellar velocity if the star is not critically rotating and some additional momentum is transferred to the circumstellar matter. Finally, in our modeling, we consider that $V_{\rm rot}$ is free with a higher maximum value equal to the critical velocity ($V_{\rm c}$).

For each target we have computed several hundreds of models to constrain the parameters, determine the uncertainties and try to detect any degeneracy or linked parameters. **Due to the large number of free-parameters, the use of an automatic model-fitting method would have resulted in the computation of millions of models. Moreover, we clearly know each parameters effects on the visibility and phases variations (see Section 5.3.2.). Consequently, we decided to perform the fit manually**. For all targets we could exclude models with significant expansion velocity of more than a few km s^{-1}. Consequently, we decided to set the expansion velocities to zero in all our models. We then tried to constrain the seven remaining parameters (i, PA, $V_{\rm rot}$, β, $a_{\rm c}$, $a_{\rm l}$, and $EW_{\rm l}$). To reduce the number of computed models, we started with a qualitative estimation of the parameters from our interferometric data (especially for PA, i, a_c, a_l and EW_l) and explore the parameter space with decreasing steps to converge to the χ^2 minimum. To check for the existence of other minima, we also explore the full range of possible parameters space but with larger steps. Finally, the parameters values for the best-fit models are presented in Table 6. The corresponding differential visibilities and phases are overplotted on Figs 3 to 10.

The fit quality is very good for three targets observed in HR mode : ω Car, μ Cen, and α Ara, and good for the two stars observed in MR mode, i.e., p Car and δ Cen. It is still satisfying for α Col (i.e. χ^2_r=4), despite the fact the visibility and phase of one of the baseline cannot be fitted simultaneously with the other ones. In the case of κ CMa, the fit is significantly worse (i.e. χ^2_r=6.8). This is mainly due to the strong asymmetry of this object that is not taken into account in our simple model. Finally, the data obtained on o Aqr seems not to be sufficient to fully constrain the model for this object (i.e. χ^2_r <1).

5.3.2. About the model parameters

To check the consistency of our modeling we tried to determine the effects of all the model parameters on the visibility and phases variations through the emission line. Some of them strongly affect the interferometric observables and are thus easily and unambiguously constrained with only a few measurements whereas others are more difficult to infer :

- the major-axis position angle (PA) has a huge effect on the phase variations amplitude and the shape of the visibility drop as already explained in Meilland et al. (2011). For a non-fully resolved disk, the amplitude of the "S" phase variation is proportional to the baseline length, but it also strongly depends on its orientation. The amplitude is maximal for baselines aligned with the major-axis and null for the one aligned with the minor-axis. For baselines overresolving the disk, the differential phase loses it simple "S" shape and secondary effects become visible (for example see the case of α Col in Fig. 4). The shape of the visibility variations also

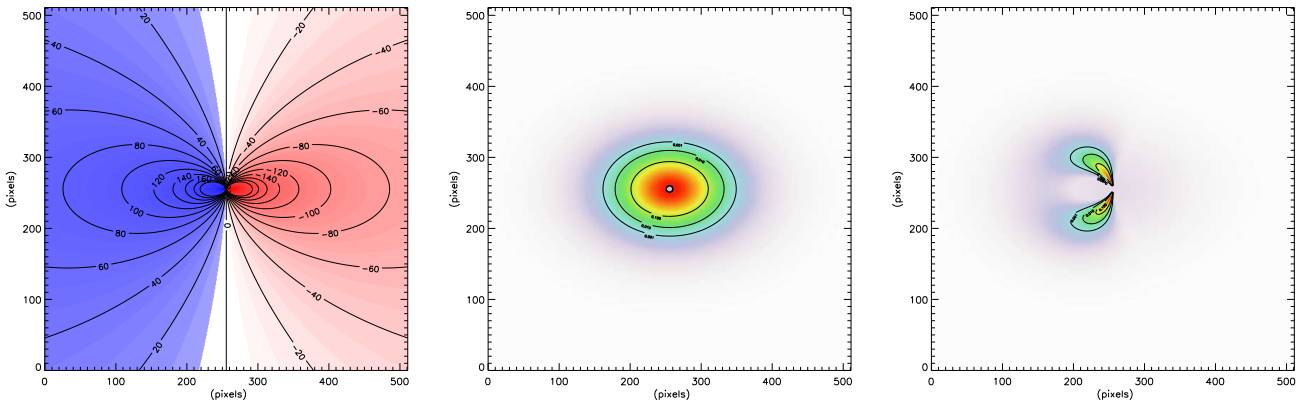

Fig. 12. Illustration of our kinematic model. Left : two-dimensional project velocity map for a purely rotating disk with an inclination angle of 45^o. The blue and red colors represents the positive and negative projected velocities, respectively. Center : global emission map in the Brγ line. It is given by a simple elliptical Gaussian with an elongation due to the projection onto the sky plane. Right : emission map in a narrow spectral channel centered around 21664Å with a resolution of 1.8Å. It is obtained using the velocity map and the emission map. See Delaa et al. (2011) for more details.

varies from "W" for baselines aligned with the major-axis to "V" for baselines aligned with the minor-axis.

- the line equivalent width (EW_l) is mainly set by the fit of the line profile. It needs to be corrected taking into account the photospheric absorption line (see Delaa et al. 2011 for more details).
- the disk FWHM in the emission line (a_l) influences the drop of visibility amplitude along all baselines and the amplitude of the "S" shape variations. It can be also constrained knowing that the phase variations lose this "S" shape for baselines that fully resolved the disk. This parameter also influences the double-peak separation : the larger is the disk, the smaller is the separation.
- the disk FWHM in the continuum (a_c) is mainly derived from the measurements in the continuum presented in Table 4. However, it also influences indirectly the amplitude of the phase variations as it can modify the ratio between the coherent flux (for an unresolved object) and the incoherent one (for a resolved object). The phase variation is proportional to the photocenter shift only for an unresolved object. Thus, the more resolved is an object in the continuum the smaller will be the phase variations. For example, in the case of α Ara, we did not manage to fit the differential phase with a disk in the continuum that extends to FWHM=3.0 mas as measured by the absolute visibility (see Table 4), but only with disks smaller than 2 mas. This may be due to a truncation of the disk, as explained in Chesneau et al. (2005) and Meilland et al (2007a), making it depart from a simple Gaussian shape.
- the inclination angle (i) has a significant influence on the visibility drop amplitude for baselines close to the polar orientation. It is well constrained by comparing equatorial and polar baselines measurements. It has also an effect on the double-peak separations since it influences the projected rotational velocity.
- the rotational velocity (V_{rot}) mainly influences the double-peak separation and the line "width". The faster the disk rotates the larger is the double-peak separation.
- the exponent of the rotation law (β) also influences the double-peak separation. With a higher value of β, the velocity as a function of the distance drop quicker and the smaller is the double-peak separation. Thus, it is quite hard to distinguish the effect of V_{rot} and β. However, β also influences the shape of wings of the line. The higher is the value of β the larger are the line wings. But, as already mentioned in Delaa et al. (2011), the wings of Be stars emission line can be highly affected by non-kinematic broadening due to non-coherent scattering, so that it remains hard to set both V_{rot} and β unambiguously. Nevertheless, value of β of less than 0.3 gives too sharp variations which are not realistic.

6. Discussions

6.1. The rotational rate of Be stars

Using the inclination angle determined from our kinematics model and the v sin i and the estimation of the critical velocity V_c from Frémat et al. (2005), we could determine the rotational velocity of the observed targets and constrain the rotational rate V/V_c. These results are presented in Table 7. In Fig. 13 we plotted the rotational rate as a function of the effective temperature to see if we find any correlation as proposed by Cranmer (2005). We did not detect any correlation between V/V_c and Teff. This striking effect could be real, or due to a small sample and our large uncertainties. Nevertheless, we found a mean rotational rate of $\overline{V/V_c}$=0.82±0.08 V_c. This value is compatible with the one determined by Frémat et al. (2005), i.e. 0.88., from their fit of photospheric lines of Be stars taking into account gravity darkening effects as proposed by Townsend et al. (2004). We note that the inclination angle determined from our modeling agrees with the one determined by Frémat et al. (2005) within 1σ for all targets except α ara (1.3σ) and α Col (2σ).

Two stars in our samples have already been studied using the VLTI/AMBER in MR mode : α Ara (Meilland et al. 2007a) and κ CMa (Meilland et al. 2007b). The inclination angle found for α Ara, i.e. 45±5^o, is roughly compatible with the previous estimation, i.e. 55^o whereas, in the case of κ CMa the two estimations are clearly not compatible, i.e. 35±5^o in this work and 60±10^o in Meilland et al. (2007b). The main differences between these previous studies and our current work is that they were conducted at the very begin of the VLTI/AMBER instrument. At this time, the uncertainties on the absolute visibility measurements where poorly known and have probably been underestimated by the authors. Unlike in the present work, they mainly used the absolute visibility measurements to determine the disk flattening and thus infer the inclination angle. Thus, their conclusion of that κ CMa rotate at about half its critical velocity is

Table 6. Best-fit parameters obtained from our axisymmetric kinematic model.

Parameter	unit	α Col	κ CMa	ω Car	p Car	δ Cen	μ Cen	α Ara	o Aqr
Global geometric parameters									
$R_\star$	($R_\odot$)	5.8	5.9	6.8	6.0	6.5	5.5	5.5	4
d	(pc)	80	202	104	148	127	155	81	133
i	(deg)	35±5	35±10	65±10	70±10	35±15	25±5	45±5	70±20
PA	(deg)	10	25±10	5±5	-25±10	40±10	80±15	88±2	120±20
Global kinematic parameters									
$V_{\rm rot}$	(km s^{-1})	350±10	480±40	300±20	400±30	500±50	510±20	480±20	400±50
β	-	0.5±0.1	0.5±0.2	0.45±0.1	0.45±0.1	0.5±0.3	0.5±0.1	0.5±0.1	0.5±0.2
K-band continuum disk geometry									
F_c	-	0.25	0.5	0.2	0.45	0.45	0.37	0.56	0.31
a_c	($D_\star$)	2.±0.5	3.5±0.5	3±1	2±0.5	2±1	<3	<2	<10
Brγ disk geometry									
a_l	($D_\star$)	5.5±0.3	6.5±2	6.5±1	11±2	9±2	4±1	5.8±0.5	14±1
EW_l	(Å)	7.0±0.5	13±2	5.8±0.5	10±1	19±2	5.6±0.3	14.5±1	12±3
χ^2_r		4.0	6.8	1.1	2.5	2.3	1.3	1.7	0.8

probably biased. Nevertheless, with its strong asymmetry due to inhomogeneity in the disk it is still hard to determine accurately κ CMa rotational velocity.

6.2. The equatorial disk extension

All the objects we have studied are, at least, partly resolved in the Brγ line. We manage to significantly constrain the extension of the line emission for all targets. We found Gaussian FWHM that range between 4 to 14 stellar diameters. We found no correlation between the Brγ emission and other properties or characteristics except the double-peaked separation (see the next subsection for the discussion on the disk kinematics.). It seems that the size is independent on the stellar parameters as well as on the infrared excess or line equivalent width. The mean FWHM of the Brγ line emission is : $6.1 \pm 2.9\,D_\star$

As already explained in Sect. 5.1, most of the targets are also partly resolved in the continuum with FWHM that range between 1.5 and 3.7 $D_\star$ and a mean FWHM of $2.2 \pm 0.3\,D_\star$. This is roughly compatible with K'-band CHARA interferometer measurements by Gies et al. (2007) on the Be stars γ Cas ($2.4\,D_\star$), ϕ Per ($3.3\,D_\star$), ζ Tau ($5.5\,D_\star$), and κ Dra ($4.3\,D_\star$).

These typical K-band continuum and Brγ line extensions are significantly smaller than the disk size measured in Hα. For example a multi-line spectro-interferometric study of the circumstellar environment of the Be star δ Sco published in Meilland et al. 2011 shows that the emission extension was 1.6 times more extended in H_α ($9\,D_\star$) than in Brγ ($5.5\,D_\star$) . Other narrow bands studies in Hα published in Tycner et al. (2004, 2006) and Quirrenbach et al. (1997) also conclude that the typical Hα extension were of the same order.

Table 7. Rotational rate of our Be stars

Star	V_c km s^{-1}	$V \sin i$ km s^{-1}	i deg	V_{star} km s^{-1}	V_{star} % of V_c
α Col	355±23	192±12	35±5	336±50	0.95±0.23
κ CMa	535±39	244±17	35±10	428±80	0.80±0.31
ω Car	320±17	245±13	65±10	270±40	0.84±0.16
p Car	401±28	285±20	70±10	303±40	0.76±0.15
δ Cen	527±29	263±14	35±15	458±100	0.87±0.41
μ Cen	508±32	155±4	25±5	369±80	0.72±0.20
α Ara	477±24	305±15	45±5	429±60	0.90±0.17
o Aqr	391±27	282±20	70±20	300±80	0.77±0.21

As explained in Meilland et al. (2007a, 2007b) using the SIMECA code (Stee et al. 1994) and Tycner et al. (2007) using the BEDISK code (Sigut & Jones 2007), these interferometric measurements can be used to constrain the circumstellar environment physical parameters : mass loss, disk mass, and temperature and density distribution. In a forthcoming paper, we will use these numerical codes and the available, V (CHARA/VEGA), K (VLTI/AMBER), and N (VLTI/MIDI) bands measurements to draw a more complete picture of the Be stars circumstellar environment.

6.3. The equatorial disk kinematics

For all our targets, the simple kinematic model reproduced very well our VLTI/AMBER measurements. Thus, it is clear that most of the Brγ line emission comes from the equatorial disk. The disk kinematics is dominated by rotation, with a rotational law close to Keplerian for all targets. The putative expansion velocity is far below the detectability limit of the instrument (i.e. <10 km s^{-1}). These results fully agree with previous kinematics studies done with the VLTI/AMBER (Meilland et al. 2007a, 2011) or CHARA/VEGA (Delaa et al. 2011).

If the disks are in Keplerian motion and the stars are rotating significantly below their critical velocity, two issues remain :

- What additional mechanisms is giving the amount of energy needed to launch the matter from the stellar surface?
- How does the ejected matter gain sufficient kinetics energy to accelerate up to the Keplerian velocity?

In other terms, the matter needs to be accelerated both radially and azimuthally. Lee et al. (1991) proposed that the disk could be formed by the effect of the gas viscosity drifting the matter outward. However, in his theory, if the star is not critically rotating, a source to supply angular momentum at the stellar surface is still needed. Non-radial pulsations as proposed by Osaki (1986) could be a good candidate. Recently, Cranmer (2009) proposed a theory in which resonant oscillations in the photosphere could inject enough angular momentum to spin up a Keplerian disk even for the slowest rotating Be stars (down to 60% of V_c). However the question remains open and other mechanisms such as magnetism (Yudin et al. 2010), radiative pressure (Abbott 1979) or binarity could also contribute to the ejection of matter. To solve the issue, the connecting layers between the stellar surface and the inner part of the equatorial disk should be

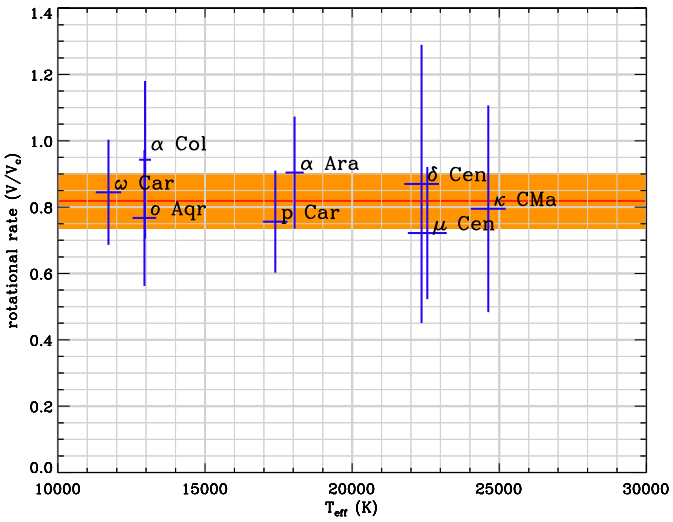

Fig. 13. The rotational rate of our Be stars sample plotted as a function of their effective temperature. Our measurements for the eight targets and their relative uncertainties are plotted as blue vertical lines. The orange box represents the mean rotational rate, i.e. 0.82±0.08.

carefully studied. This could be done by studying many absorption and emission lines formed close to the photosphere and by comparing their morphology.

6.4. Departures from our simple model

Despite the globally good fit of our interferometric data using the simple kinematic model, there is two significant departures from the model that need to be investigated:

- The most important one is the case of κ CMa that is clearly showing asymmetric profile and visibility and phase variations. Such asymmetries can only originate from the presence of inhomogeneities in the circumstellar environment. To determine whether or not these inhomogeneities can be modeled as one-armed oscillations as proposed by Okazaki (1997) a dedicated model need to be developed. Such thorough analysis of κ CMa data is out of the scope of this paper. We note that despite the lower resolution the p Car data are also showing clues of the same kind of asymmetries.
- The second most important departure from the model concerns the measurement obtained on α Col with the short polar baseline that cannot be fitted simultaneously with the other ones. This measurement shows that the environment is almost fully resolved with B≃27 m for this orientation, whereas it is clearly less extended with a baseline closer to the equator. This could be a clue of the presence of a polar wind as already detected by Kervella & Domiciano de Souza (2006) on the classical Be star Achernar. However, a detailed study of the circumstellar environment of Be stars along their polar axis is needed to definitively answer the question of the detectability of polar winds in the K-band (see Stee 2011 for a detail discussion on the polar winds of Be stars).

These two issues on the circumstellar environments of Be stars will be studied in details in some forthcoming dedicated papers.

7. Conclusion

In this spectro-interferometric survey of classical Be stars we managed to resolve all targets, constrain their extension in the Brγ line and, for some of them, in the K-band continuum. Using a simple kinematic model of a purely rotating disk, we were able to successfully model all our data, showing that most of the Brγ emission originates from the equatorial region. The disk is fully dominated by rotation, and the rotation law was found to be Keplerian or quasi-Keplerian for all targets. We were also able to significantly constrain the stellar rotational velocity using our estimation of the inclination angle. We found a mean rotation rate of V/V$_c$= 0.82±0.08 which is compatible with previous estimation by Frémat et al.(2005) done by modeling photospheric lines.

We did not detect any correlation between the stellar parameters and the disk properties. However, the uncertainties on the measurements remains high and our sample of Be star need to be extended to definitively answer the issue on the physical process or processes responsible for the mass ejection and the dependence of the Be phenomenon on the stellar parameters.

In a forthcoming paper, these data will be analyzed using the radiative transfer codes SIMECA and BEDISK in order to fully constrain the circumstellar environment.

Acknowledgements. The Programme National de Physique Stellaire (PNPS) and the Institut National en Sciences de l'Univers (INSU) are acknowledged for their financial supports. S. Kanaan also acknowledges financial support from the GEMINI-CONICYT Fund, allocated to the project N 32090006.

References

Abbott D.C., 1979, IAUS, 83, 237A
Borges Fernandes M., Meilland A., Bendjoya P. et al. 2011, A&A, 528, 20
Cranmer S.R., 2005, ApJ, 634, 585
Cranmer S.R., 2009, ApJ, 701, 413
Delaa, O., Stee, Ph., Meilland, A. et al. 2011, A&A, 529, A163
Domiciano de Souza, A., Kervella, P., Jankov, S., et al. 2003, A&A, 407, L47
Frémat Y, Zorec J, Hubert A.-M. & Floquet M. 2005 A&A, 440, 305
Gies, D.R., Bagnuolo, W.G., Baines, E.K. et al. 2007, ApJ, 654, 527
Kervella P. & Domiciano de Souza A. 2006, A&A, 453, 1059
Kurucz, R.L. 1979, ApJ, 40, 1
Lamers H.J.G.L.M. & Waters L.B.F.M. 1987, A&A, 182, 80
Leinert C., Graser U., Waters, L.B. et al. 2003, SPIE 4006, 43
Marlborough J.M 1982, IAUS, 98, 361
Meilland A., Stee, P., Vannier M., et al. 2007a, A&A, 464, 59
Meilland A., Millour F., Stee Ph., et al. 2007b, a&A, 464, 73
Meilland A., Millour F., Stee Ph., et al. 2008, A&A, 488, 67L
Meilland, A., Stee, Ph. Chesneau, O. et al. 2009, A&A, 505, 687
Meilland A., Kanaan S., Borges Fernandes M. et al. 2010, A&A, 512, 73
Meilland A., Delaa O., Stee Ph., et al. 2011, A&A, 532, 80
Millour F., Petrov R.G., Chesneau O. et al., 2007, A&A, 464, 107
Millour F. Chesneau O., Borges Fernandes M., et al. 2009, A&A, 507, 317
Millour F., Meilland A., Chesneau O. et al. 2011, A&A, 526, 107
Mourard D., Clausse, J.M., Marcotto, A. et al. 2009, A&A, 508, 1073
Okazaki A.T., 1997, A&A, 318,548
Petrov, R.G. et al., 2007, A&A , 464, 1
Quirrenbach A., Bjorkman K.S., Bjorkman J.E.et al. 1997, ApJ, 479, 477
Robbe-Dubois S., Lagarde S., Petrov R.G. et al., A&A, 464, 13
Schaefer, G.H., Gies, D.R., Monnier, J.D. et al. 2010, RevMexAA (serie de Conferencias), 38, 107
Sigut, T.A.A. & Jones, C.E., 2007, ApJ, 668, 481
Stee Ph. & de Ajaújo F.X. 1994, A&A, 292, 221
Stee, Ph. & Meilland A., 2009, Lectures notes in Physics, 765, 195
Stee Ph. 2011, IAUS, 272, 313
Tatulli E., Millour F., Chelli A et al. 2007, 464, 29
Townsend R.H., Owocki S.P., & Howard I.D., 2004, MNRAS 350, 189
Tycner C., Hajian A.R., Armstrong J.T.et al. , 2004, AJ, 127, 194
Tycner, C., Gilbreath, G.C., Zavala, R.T. et al. 2006, AJ, 131, 2710
Tycner, C., Jones, C.E., Sigut, T.A.A. et al. 2008, ApJ, 689, 461
van Leeuwen F. 2007, Astrophysics and Space Science Library,volume 350, Hipparcos the new reduction of the raw data (Springer)

Yudin R.V, A&A, 2001, 368, 912
Yudin R.V., Hubrig S., Pogodin M.A. 2010, IAUS, 272, 224
Waters, L. B. F. M. 1986, A&A, 162, 121
Wisniewksi, J.P., Kowalski, A.F., Bjorkman, K.S. et al. 2007, ApJ, 656, L21